

Discovery limits for techni-omega production in $e\gamma$ collisions

Stephen Godfrey

Ottawa-Carleton Institute for Physics, Department of Physics, Carleton University, Ottawa, Canada K1S 5B6

Tao Han

Department of Physics, University of Wisconsin, Madison, Wisconsin 53706

Pat Kalyniak

Ottawa-Carleton Institute for Physics, Department of Physics, Carleton University, Ottawa, Canada K1S 5B6

(Received 27 October 1998; published 1 April 1999)

In a strongly interacting electroweak sector with an isosinglet vector state, such as the techni-omega, ω_T , the direct $\omega_T Z \gamma$ coupling implies that an ω_T can be produced by $Z \gamma$ fusion in $e\gamma$ collisions. This is a unique feature for high energy e^+e^- or e^-e^- colliders operating in an $e\gamma$ mode. We consider the processes $e^- \gamma \rightarrow e^- Z \gamma$ and $e^- \gamma \rightarrow e^- W^+ W^- Z$, both of which proceed via an intermediate ω_T . We find that at a 1.5 TeV e^+e^- linear collider operating in an $e\gamma$ mode with an integrated luminosity of 200 fb^{-1} , an ω_T can be discovered for a broad range of masses and widths. [S0556-2821(99)03209-9]

PACS number(s): 12.60.-i, 12.60.Nz, 14.80.-j

I. INTRODUCTION

The mechanism for electroweak symmetry breaking remains the most prominent mystery in elementary particle physics. In the standard model (SM), a neutral scalar fundamental Higgs boson is expected with a mass (m_H) less than about 800 GeV. In the weakly coupled supersymmetric extension of the SM, the lightest Higgs boson is expected to be lighter than about 140 GeV. Searching for the Higgs bosons is a primary goal of current and future collider experiments [1]. However, if no light fundamental Higgs boson is found for $m_H < 800$ GeV, one would anticipate that the interactions among the longitudinal vector bosons become strong [2]. This is the case when strongly interacting dynamics is responsible for electroweak symmetry breaking, such as in technicolor models [3].

Without knowing the underlying dynamics of the strongly interacting electroweak sector (SEWS), it is instructive to parametrize the physics with an effective theory for the possible low-lying resonant states. This typically includes an isosinglet scalar meson (H) and an isotriplet vector meson (ρ_T) [4]. However, in many dynamical electroweak symmetry breaking models there exist other resonant states such as an isosinglet vector (ω_T), and isotriplet vector (a_{1T}) [5,6]. In fact it has been argued that to preserve good high energy behavior for strong scattering amplitudes in a SEWS, it is necessary for all the above resonant states to coexist [7]. It is therefore wise to keep an open mind and to consider other characteristic resonant states when studying the physics of a SEWS at high energy colliders.

Among those heavy resonant states, the isosinglet vector state ω_T has rather unique features. Because of its isosinglet nature, it does not have strong coupling to two gauge bosons. It couples strongly to three longitudinal gauge bosons $W_L^+ W_L^- Z_L$ (or equivalently, electroweak Goldstone bosons $w^+ w^- z$) and electroweakly to $Z \gamma$, ZZ , and $W^+ W^-$. It may mix with the $U(1)$ gauge boson B , depending on its hyper-

charge assignment in the model. The signal for ω_T production was studied for pp collisions at 40 TeV and 17 TeV [5,6]. It appears to be difficult to observe the ω_T signal at the CERN Large Hadron Collider (LHC), largely due to the SM backgrounds. On the other hand, the direct $\omega_T Z_L \gamma$ coupling implies that an ω_T can be effectively produced by $Z_L \gamma$ fusion in $e\gamma$ collisions. This is a unique feature for high energy e^+e^- or e^-e^- colliders operating in an $e\gamma$ mode. In this paper we concentrate on ω_T production at $e\gamma$ linear colliders. We first describe a SEWS scenario in Sec. II in terms of an effective Lagrangian involving ω_T interactions. We then present our results in Sec. III for the production and decay of an ω_T in $e\gamma$ colliders. We show that a high energy $e\gamma$ linear collider will have great potential for the discovery of an ω_T with a mass of order 1 TeV. We conclude in Sec. IV.

II. ω_T INTERACTIONS

For an isosinglet vector, a techniomega-like state ω_T , the leading strong interaction can be parametrized by

$$\mathcal{L}_{\text{strong}} = \frac{g_\omega}{v\Lambda^2} \varepsilon_{\mu\nu\rho\sigma} \omega_T^\mu \partial^\nu w^+ \partial^\rho w^- \partial^\sigma z, \quad (1)$$

where $v = 246$ GeV is the scale of electroweak symmetry breaking and Λ is the new physics scale at which the strong dynamics sets in. The effective coupling g_ω is of strong coupling strength, and is model-dependent. It governs the partial decay width $\Gamma(\omega_T \rightarrow w^+ w^- z) \equiv \Gamma_{WWZ}$. To study the ω_T signal in a model-independent way, we will use this physical partial width as the input parameter to extract the factor ($g_\omega/v\Lambda^2$). With the interaction Eq. (1), the spin-averaged amplitude squared for the decay $\omega_T \rightarrow W^+ W^- Z$ is calculated to be

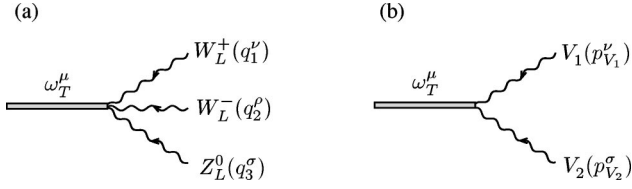


FIG. 1. Effective interactions of ω_T with (a) w^+w^-z and (b) two vector bosons.

$$\begin{aligned} & \bar{\Sigma} |\mathcal{M}(\omega_T \rightarrow WWZ)|^2 \\ &= \frac{1}{3} \frac{g_\omega^2}{v^2 \Lambda^4} \{ M_W^4 M_Z^2 + 2q_1 \cdot q_2 q_2 \cdot q_3 q_3 \cdot q_1 \\ & \quad - M_Z^2 (q_1 \cdot q_2)^2 - M_W^2 ((q_2 \cdot q_3)^2 + (q_1 \cdot q_3)^2) \}. \end{aligned}$$

The four-momenta in this expression correspond to the labeling of Fig. 1(a). As the full expression for Γ_{WWZ} is rather complicated, we evaluated the phase space integral numerically to relate $(g_\omega/v\Lambda^2)$ to Γ_{WWZ} .

The effective Lagrangian describing the electroweak interactions of the ω_T with the electroweak gauge bosons can be written as [5]

$$\begin{aligned} \mathcal{L}_{\text{e.w.}} = & \chi \varepsilon_{\mu\nu\rho\sigma} \left[-g \text{Tr} \left(\frac{\vec{\sigma}}{2} \cdot \vec{W}^{\rho\sigma} \{ \Sigma D^\nu \Sigma^\dagger, \omega_T^\mu \} \right) \right. \\ & \left. + g' \text{Tr} \left(\frac{\sigma^3}{2} B^{\rho\sigma} \{ \Sigma^\dagger D^\nu \Sigma, \omega_T^\mu \} \right) \right], \end{aligned} \quad (2)$$

where the covariant derivative is defined by

$$D^\mu \Sigma = \partial^\mu \Sigma - ig \vec{W}^\mu \cdot \frac{\vec{\sigma}}{2} \Sigma + ig' \Sigma B^\mu \frac{\sigma_3}{2}, \quad (3)$$

g and g' are the $SU(2)_L$ and $U(1)_Y$ coupling constants, Σ is the non-linearly realized representation of the Goldstone boson fields and transforms like $\Sigma \rightarrow L \Sigma R^\dagger$. In the unitary gauge $\Sigma \rightarrow 1$. With these substitutions $\mathcal{L}_{\text{e.w.}}$ leads to

$$\begin{aligned} \mathcal{L}_{\text{e.w.}} \sim & 2ie^2 \chi \varepsilon_{\mu\nu\rho\sigma} \omega_T^\mu \left[\frac{1}{\sin^2 \theta_w} (\partial^\rho W^{+\sigma} W^{-\nu} + \partial^\rho W^{-\sigma} W^{+\nu}) \right. \\ & + \left(\frac{\cos^2 \theta_w}{\sin^2 \theta_w} - \frac{\sin^2 \theta_w}{\cos^2 \theta_w} \right) \partial^\rho Z^\sigma Z^\nu \\ & \left. + \frac{2}{\sin \theta_w \cos \theta_w} \partial^\rho \gamma^\sigma Z^\nu \right] + \dots \end{aligned} \quad (4)$$

where θ_w is the electroweak mixing angle. The last term gives the $\omega_T Z \gamma$ vertex, of importance for production of the ω_T in $e\gamma$ colliders. It involves the unknown coupling parameter χ , where $e\chi^{1/2}$ is expected to be of electroweak strength. Similarly, the $\omega_T W^+ W^-$ and $\omega_T ZZ$ vertices, corresponding to the first and second terms, respectively, of Eq. (4) above, are proportional to χ . The Feynman rules for the effective

TABLE I. Feynman rules for the effective interactions of ω_T .

Vertex	Feynman rule
$\omega_T w^+ w^- z$	$ig_{\omega_T}/(v\Lambda^2) \varepsilon_{\mu\nu\rho\sigma} \epsilon^\mu(\omega) q_1^\nu q_2^\rho q_3^\sigma$
$\omega_T Z \gamma$	$i4e^2 \chi / (\sin \theta_w \cos \theta_w) \varepsilon_{\mu\nu\rho\sigma} \epsilon^\mu(\omega) \epsilon^\nu(Z) p_2^\rho \epsilon^\sigma(\gamma)$
$\omega_T ZZ$	$i4e^2 \chi (\cot^2 \theta_w - \tan^2 \theta_w) \varepsilon_{\mu\nu\rho\sigma} \epsilon^\mu(\omega) \epsilon_1^\nu p_2^\rho \epsilon_2^\sigma$
$\omega_T W^+ W^-$	$i2e^2 \chi / \sin^2 \theta_w \varepsilon_{\mu\nu\rho\sigma} \epsilon^\mu(\omega) \epsilon_-^\nu (p_+^\rho - p_-^\rho) \epsilon_+^\sigma$

interactions of the ω_T , represented in Fig. 1, are given in Table I. We take the partial width of the ω_T into these two body states,

$$\Gamma_{2\text{-body}} = \Gamma(\omega_T \rightarrow Z\gamma) + \Gamma(\omega_T \rightarrow W^+W^-) + \Gamma(\omega_T \rightarrow ZZ)$$

as input to determine this coupling χ . The two body partial widths are

$$\begin{aligned} \Gamma(\omega_T \rightarrow Z\gamma) = & \frac{8\pi\alpha^2\chi^2}{3\cos^2\theta_w\sin^2\theta_w} \frac{M_{\omega_T}^3}{M_Z^2} \left(1 - \frac{M_Z^2}{M_{\omega_T}^2} \right)^3 \\ & \times \left(1 + \frac{M_Z^2}{M_{\omega_T}^2} \right), \end{aligned} \quad (5)$$

$$\begin{aligned} \Gamma(\omega_T \rightarrow W^+W^-) = & \frac{4\pi\alpha^2\chi^2}{3\sin^4\theta_w} \frac{M_{\omega_T}^3}{M_W^2} \sqrt{1 - 4\frac{M_W^2}{M_{\omega_T}^2}} \\ & \times \left(1 - 4\frac{M_W^2}{M_{\omega_T}^2} \right)^2, \end{aligned} \quad (6)$$

$$\begin{aligned} \Gamma(\omega_T \rightarrow ZZ) = & \frac{8\pi\alpha^2\chi^2}{3} (\cot^2\theta_w - \tan^2\theta_w)^2 \\ & \times \frac{M_{\omega_T}^3}{M_Z^2} \sqrt{1 - 4\frac{M_Z^2}{M_{\omega_T}^2}} \\ & \times \left[6\frac{M_Z^4}{M_{\omega_T}^4} + \frac{1}{2} \left(1 + \frac{M_Z^2}{M_{\omega_T}^2} \right) \left(1 - 4\frac{M_Z^2}{M_{\omega_T}^2} \right) \right]. \end{aligned} \quad (7)$$

III. CALCULATION AND RESULTS

We consider the two signal processes which proceed via an intermediate ω_T :

$$e^- \gamma \rightarrow e^- \omega_T \rightarrow e^- Z \gamma, \quad (8)$$

$$e^- \gamma \rightarrow e^- \omega_T \rightarrow e^- W^+ W^- Z. \quad (9)$$

Depending upon the $\omega_T Z \gamma$ coupling, the signal cross section can be fairly large. The cross section expressions are lengthy and we do not present them here. We choose to look at these $Z\gamma$ and WWZ final states based on the distinctive signature

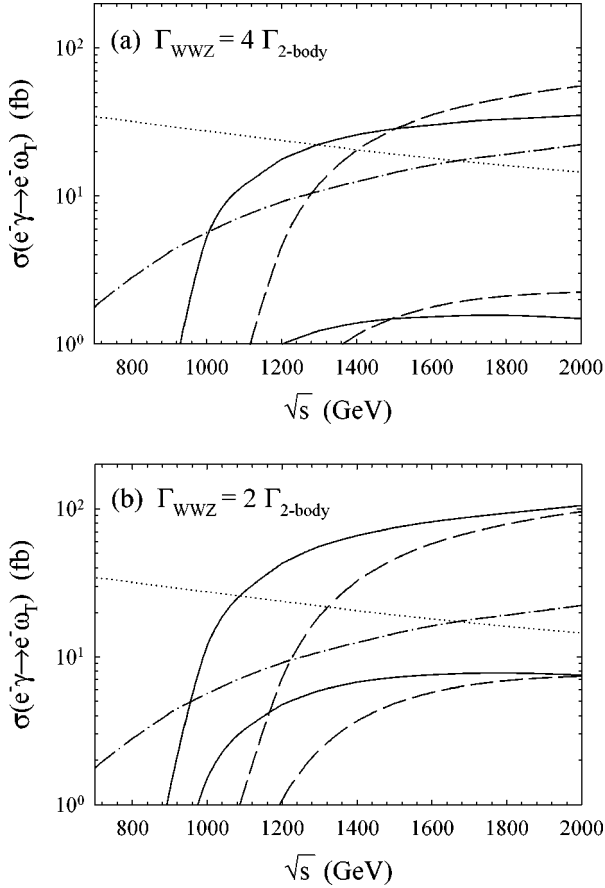


FIG. 2. Cross sections versus the e^+e^- c.m. energy for the signal $e^-\gamma \rightarrow e^-\omega_T$ with $\omega_T \rightarrow W^+W^-Z$ and $Z\gamma$ and the SM backgrounds. The solid lines are for $M_{\omega_T} = 0.8$ TeV and the long-dashed lines for $M_{\omega_T} = 1.0$ TeV. In each case the curve with the larger cross section is for the W^+W^-Z final state and the lower for the $Z\gamma$ final state. The dash-dot line is for the $e^-W^+W^-Z$ SM background and the dotted line is for the $e^-Z\gamma$ SM background. In (a), $\Gamma_{WWZ} = 4\Gamma_{2\text{-body}}$, and in (b), $\Gamma_{WWZ} = 2\Gamma_{2\text{-body}}$. The chosen values of the partial widths are given in the text.

of the first process and the potential enhancement of the second arising from its dependence on the strong coupling g_ω .

The SM background to the process $e\gamma \rightarrow eZ\gamma$ is the bremsstrahlung of photons and Z 's from the electron. The background process to the $e^-W^+W^-Z$ final state has a complicated structure, with 90 diagrams. The main contribution comes from the subprocesses $e^+e^- \rightarrow W^+W^-$, $\gamma\gamma \rightarrow W^+W^-$ with a radiated Z . We use the MADGRAPH package [8] to evaluate the full SM amplitudes for the background processes.

In calculating the total cross sections for the $eZ\gamma$ signal and the backgrounds, we impose the following ‘‘basic cuts’’ to roughly simulate the detector coverage:

$$\begin{aligned} 170^\circ > \theta_e > 10^\circ, \quad 165^\circ > \theta_\gamma > 15^\circ, \\ \theta_{e\gamma} > 30^\circ, \quad E_\gamma > 50 \text{ GeV}, \end{aligned} \quad (10)$$

where θ_e is the polar angle with respect to the e^- beam direction in the lab (e^+e^- c.m.) frame and $\theta_{e\gamma}$ is the angle

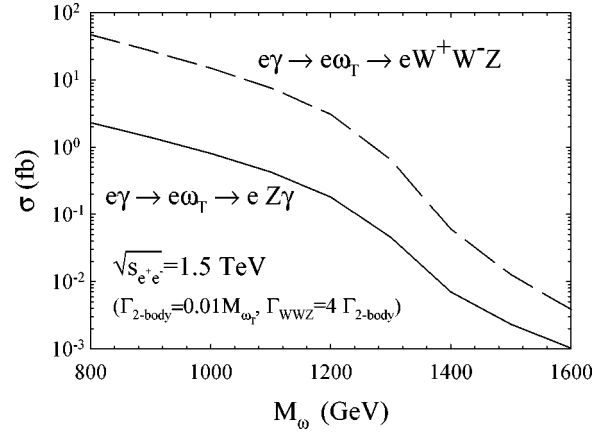


FIG. 3. Cross sections versus the M_{ω_T} for the signal $e^-\gamma \rightarrow e^-\omega_T$ for $\sqrt{s_{e^+e^-}} = 1.5$ TeV with $\omega_T \rightarrow W^+W^-Z$ (dashed line) and $Z\gamma$ (solid line).

between the outgoing e^- and γ . Only the cut on θ_e is relevant to the $e^-W^+W^-Z$ process. The cuts on photons also regularize the infrared and collinear divergences in the tree-level background calculations.

We have also implemented the back-scattered laser spectrum for the photon beam [9]. For simplicity, we have ignored the possible polarization for the electron and photon beams, although an appropriate choice of photon beam polarization may enhance the signal and suppress the backgrounds.

We present the total cross section for the signal and background versus the e^+e^- c.m. energy $\sqrt{s_{e^+e^-}}$ in Fig. 2 with various choices of ω_T mass and partial widths. We have taken representative values for M_{ω_T} of 0.8 (1.0) TeV. In Fig. 2(a), we use partial widths $\Gamma_{2\text{-body}} = 5$ (20) GeV and $\Gamma_{WWZ} = 20$ (80) GeV, setting $\Gamma_{WWZ} = 4\Gamma_{2\text{-body}}$. In Fig. 2(b), we take $\Gamma_{2\text{-body}} = 15$ (40) GeV and $\Gamma_{WWZ} = 30$ (80) GeV, such that $\Gamma_{WWZ} = 2\Gamma_{2\text{-body}}$. As noted above, the values for the couplings χ and g_ω are obtained using these partial widths as input. In Fig. 2(b), the 2-body decay modes represent a larger fraction of the total width and, hence, the cross sections for the signal processes, which go via $Z\gamma$ fusion, are enhanced due to the larger value of χ . We see that, for the parameters considered, the signal cross sections for the $e^-W^+W^-Z$ channel are about 10–100 fb once above the ω_T mass threshold and overtake the background rates by as much as an order of magnitude. Such high production rates imply that the linear collider would have great potential to discover and study the ω_T . The cross sections for the $Z\gamma$ final state are lower, as expected, and lie below the background when only the cuts of Eq. (10) are imposed.

The reason that the cross section for $M_{\omega_T} = 1.0$ TeV becomes larger than that for 0.8 TeV in Fig. 2(a) is because we have chosen relatively larger couplings for the 1.0 TeV ω_T , based on the larger input partial widths.

In Fig. 3, we show the total signal cross sections versus M_{ω_T} for $\sqrt{s_{e^+e^-}} = 1.5$ TeV. The couplings are the values

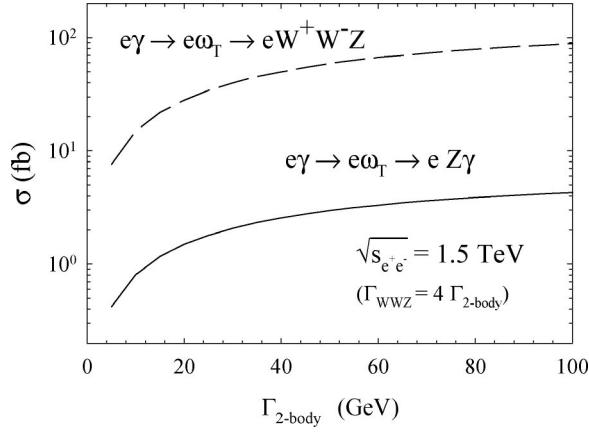


FIG. 4. Cross sections versus the partial width $\Gamma_{2\text{-body}}$ for the signal $e^- \gamma \rightarrow e^- \omega_T \rightarrow e W^+ W^- Z$ (dashed line) and $Z \gamma$ (solid line). For $\sqrt{s_{e^+e^-}} = 1.5$ TeV and $M_{\omega_T} = 1$ TeV with $\omega_T \rightarrow W^+ W^- Z$ (dashed line) and $Z \gamma$ (solid line).

obtained by taking $\Gamma_{2\text{-body}} = 1\% M_{\omega_T}$ and $\Gamma_{WWZ} = 4\Gamma_{2\text{-body}}$. As expected, below the mass threshold $\sqrt{s_{e\gamma}} < M_{\omega_T}$, the signal cross section drops sharply. However, depending on the broadness of the resonance, there is still non-zero signal cross section.

We have chosen partial decay widths of ω_T as input parameters to characterize its coupling strength. It is informative to explore how the cross section changes with the widths. Figure 4 demonstrates this point, for $\sqrt{s_{e^+e^-}} = 1.5$ TeV and $M_{\omega_T} = 1$ TeV. We vary $\Gamma_{2\text{-body}}$ and take $\Gamma_{WWZ} = 4\Gamma_{2\text{-body}}$. Measurement of the signal cross section rates and relative branching fractions for the two channels would reveal important information on the underlying SEWS dynamics.

Although the SM backgrounds seem to be larger or, at best comparable, to the signal rate for the $Z\gamma$ channel, the final state kinematics is very different between them. Because the final state vector bosons in the signal are from the

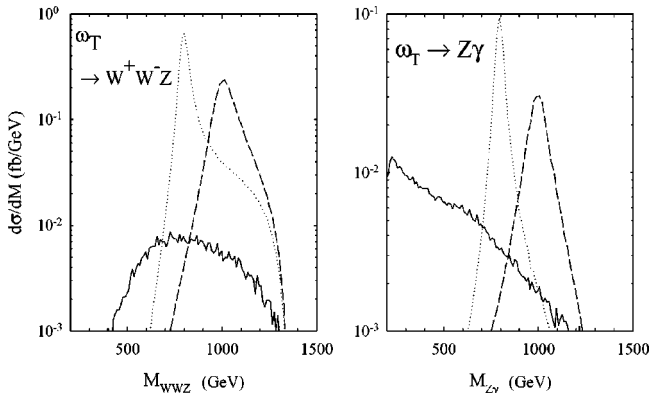


FIG. 5. Differential cross sections for $\sqrt{s_{e^+e^-}} = 1.5$ TeV as a function of the invariant mass of the ω_T decay products $M(WWZ)$ and $M(Z\gamma)$ for the signal $e^- \gamma \rightarrow e^- \omega_T$ with $\omega_T \rightarrow W^+ W^- Z$ and $Z\gamma$. The dotted lines are for $M_{\omega_T} = 0.8$ TeV ($\Gamma_{\omega_T} = \Gamma_{2\text{-body}} + \Gamma_{WWZ} = 15 + 30$ GeV) and the dashed lines for $M_{\omega_T} = 1.0$ TeV ($\Gamma_{\omega_T} = 40 + 80$ GeV). The SM background relevant to each case is given by the solid lines.

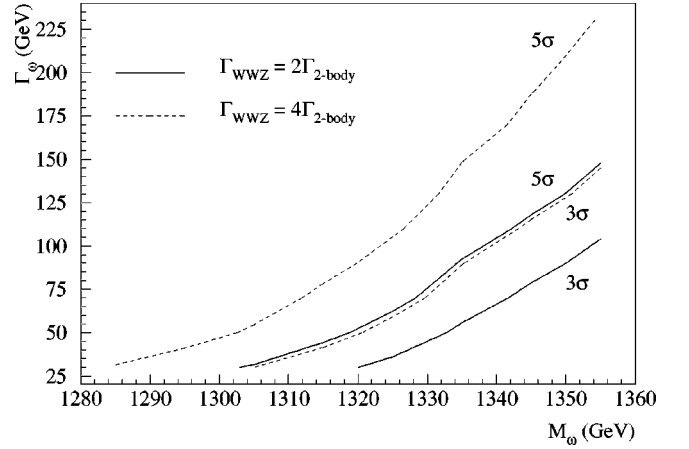


FIG. 6. Contours representing 3σ and 5σ ω_T discovery limits in the parameter space for M_{ω_T} and Γ_{ω_T} with $\sqrt{s_{e^+e^-}} = 1.5$ TeV and an integrated luminosity of 200 fb^{-1} . Two choices of the ratio of Γ_{WWZ} to $\Gamma_{2\text{-body}}$ are shown.

decay of a very massive particle, they are generally very energetic and fairly central. We thus impose further cuts to reduce the backgrounds at little cost to the signal:

$$15^\circ < \theta_{\gamma,Z,W} < 165^\circ, \quad E_{\gamma,Z,W} > 150 \text{ GeV}. \quad (11)$$

The most distinctive feature for the signal is the resonance in the invariant mass spectrum for W^+W^-Z and $Z\gamma$ final states. We demonstrate this in Fig. 5 for both the W^+W^-Z and $Z\gamma$ modes. Results for M_{ω_T} of 0.8 TeV (dotted lines) and 1.0 TeV (dashed lines) are shown for $\sqrt{s_{e^+e^-}} = 1.5$ TeV. We take $\Gamma_{WWZ} = 2\Gamma_{2\text{-body}}$. The cuts in both Eqs. (10) and (11) are imposed. We see that a resonant structure at M_{ω_T} is evident and the SM backgrounds (solid lines) after cuts (11) are essentially negligible for the particular choice of parameters shown.

To further assess the discovery potential, we explore the parameter space for M_{ω_T} and Γ_{ω_T} at a 1.5 TeV linear collider. The signal for the WWZ mode consists of both W 's decaying hadronically and the Z decaying hadronically or into electrons or muons. The same Z decay modes provide the signal for the $Z\gamma$ channel, along with the detected photon. We assume an 80% detection efficiency for each of the W , Z , and γ and an integrated luminosity of 200 fb^{-1} . In Fig. 6, we give contours representing 3σ and 5σ discovery limits for the two cases of $\Gamma_{WWZ} = 2\Gamma_{2\text{-body}}$ (solid lines) and $\Gamma_{WWZ} = 4\Gamma_{2\text{-body}}$ (dashed lines). For these results, both cuts (10) and (11) are imposed. In addition, a cut about the invariant masses M_{WWZ} , $M_{Z\gamma} \pm \Gamma_{\omega_T}$ is made for the signals and backgrounds. The two channels are combined by convolution of the product of their respective Gaussian probability functions. We present the results for the techniomega mass and width range at the limit of its resonance production at a 1.5 TeV collider. As an example, from Fig. 6, we see that for Γ_{ω_T} of 100 GeV, an ω_T can be detected at the 3σ level up to M_{ω_T} of about 1340 GeV for $\Gamma_{WWZ} = 4\Gamma_{2\text{-body}}$ and up to 1355 GeV for $\Gamma_{WWZ} = 2\Gamma_{2\text{-body}}$.

IV. CONCLUSIONS

A high energy $e\gamma$ collider is unique in producing an isosinglet vector state such as ω_T . We calculated the signal cross sections for processes (8) and (9) in an effective Lagrangian framework. We found that signal rates can be fairly large once above the M_{ω_T} threshold, although the determining factor is the effective electroweak coupling of the ω_T , parametrized by χ . The signal characteristics are very different from the SM backgrounds, making the discovery and further study of ω_T physics very promising at the linear collider. With an integrated luminosity of 200 fb^{-1} at $\sqrt{s_{e^+e^-}}$

$= 1.5 \text{ TeV}$, one may discover an ω_T for a broad range of masses and widths, as indicated in Fig. 6.

ACKNOWLEDGMENTS

This research was supported in part by the Natural Sciences and Engineering Research Council of Canada, and in part by the U.S. Department of Energy under Grant No. DE-FG02-95ER40896. Further support for T.H. was provided by the University of Wisconsin Research Committee, with funds granted by the Wisconsin Alumni Research Foundation. P.K. thanks Dean Karlen and Bob Carnegie for useful discussions.

-
- [1] For recent reviews on weakly coupled electroweak sector, see e.g., H.E. Haber, T. Han, F. Merritt, and J. Womersley, in *New Directions in High Energy Physics*, Proceedings of the Snowmass Summer Study, Snowmass, Colorado, 1996, edited by D. Cassel *et al.* (SLAC, Stanford, 1997), hep-ph/9703391; *Perspectives on Higgs Physics II*, edited by Gordon L. Kane (World Scientific, Singapore, 1997).
- [2] For recent reviews on strongly coupled electroweak sector, see, e.g., R.S. Chivukula, M.J. Dugan, M. Golden, and E.H. Simmons, *Annu. Rev. Nucl. Part. Sci.* **45**, 255 (1995); T. Barklow *et al.*, in *New Directions in High Energy Physics* [1], hep-ph/9704217; T. Han, Tegernsee 1996, The Higgs Puzzle, Ringberg, Germany, 1996, p. 197, hep-ph/9704215.
- [3] For a modern review on technicolor theories, see, i.e., K. Lane, in *ICHEP'96*, Proceedings of the 28th International Conference, Warsaw, Poland, edited by Z. Ajduk and A. Wroblewski (World Scientific, Singapore, 1997), p. 367.
- [4] See for example, M. Golden, T. Han, and G. Valencia, in *Electroweak Symmetry Breaking and New Physics at the TeV Scale*, edited by T.L. Barklow, S. Dawson, H.E. Haber, and J.L. Siegrist (World Scientific, Singapore, 1996), p. 292, hep-ph/9511206 and references therein; J. Bagger, V. Barger, K. Cheung, J. Gunion, T. Han, G. Ladinsky, R. Rosenfeld, and C.P. Yuan, *Phys. Rev. D* **49**, 1246 (1994); **52**, 3878 (1995).
- [5] R.S. Chivukula and M. Golden, *Phys. Rev. D* **41**, 2795 (1990).
- [6] R. Rosenfeld and J. Rosner, *Phys. Rev. D* **38**, 1530 (1988); R. Rosenfeld, *ibid.* **39**, 971 (1989).
- [7] T. Han, Z. Huang, and P.Q. Hung, *Mod. Phys. Lett. A* **11**, 1131 (1996).
- [8] T. Stelzer and W. Long, *Comput. Phys. Commun.* **81**, 357 (1994)
- [9] I.F. Ginzburg *et al.*, *Nucl. Instrum. Methods Phys. Res.* **205**, 47 (1983); **219**, 5 (1984). C. Akerlof, Ann Arbor Report No. UM HE 81-59, 1981 (unpublished).